Evaluation of a pixelated large format CMOS sensor for x-ray microbeam radiotherapy

Samuel Flynn[a),1,2], Tony Price[1,2] and Phil Allport[1]

Ileana Silvestre Patallo[2,3], Russell Thomas[2] and Anna Subiel[2]

Stefan Bartzsch[4,5], Franziska Treibel[5] and Mabroor Ahmed[5]

Jon Jacobs-Headspith[6], Tim Edwards[6], Isaac Jones[6] and Dan Cathie[6]

Nicola Guerrini[7] and Iain Sedgwick[7]

[1]*School of Physics and Astronomy, University of Birmingham, Birmingham, B15 2TT, United Kingdom*

[2]*Medical Physics department, National Physical Laboratory, Teddington, TW11 0LW, United Kingdom*

[3]*UCL Cancer Institute, University College London, London, WC1E 6AG, United Kingdom*

[4]*Helmholtz Centre Munich, Institute for Radiation Medicine, Munich, 85764, Germany*

[5]*Technical University of Munich, School of Medicine, Klinikum rechts der Isar, Department of Radiation Oncology, Munich, 80333, Germany*

[6]*vivaMOS Ltd, Southampton, SO16 7NP, United Kingdom*

[7]*Rutherford Appleton Laboratory, OX11 0QX, Oxford, United Kingdom*

Purpose: Current techniques and procedures for dosimetry in microbeams typically rely on radiochromic film or small volume ionisation chambers for validation and quality assurance in 2D and 1D, respectively. Whilst well characterised for clinical and preclinical radiotherapy, these methods are non-instantaneous and do not provide real time profile information. The objective of this work is to determine the suitability of the newly developed vM1212 detector, a pixelated CMOS (complementary metal-oxide-semiconductor) imaging sensor, for *in situ* and *in vivo* verification of x-ray microbeams.

Methods: Experiments were carried out on the vM1212 detector using a 220 kVp small animal radiation research platform (SARRP) at the Helmholtz Centre Munich. A 3 x 3 cm^2 square piece of EBT3 film was placed on top of a marked non-fibrous card overlaying the sensitive silicon of the sensor. 1 cm of water equivalent bolus material was placed on top of the film for build-up. The response of the detector was compared to an Epson Expression 10000XL flatbed scanner using FilmQA Pro with triple channel dosimetry. This was also compared to a separate exposure using 450 µm of silicon as a surrogate for the detector and a Zeiss Axio Imager 2 microscope using an optical microscopy method of dosimetry. Microbeam collimator slits with range of nominal widths of 25, 50, 75 and 100 µm were used to compare

beam profiles and determine sensitivity of the detector and both film measurements to different microbeams.

Results: The detector was able to measure peak and valley profiles in real-time, a significant reduction from the 24 hour self-development required by the EBT3 film. Observed full width at half maximum (FWHM) values were larger than the nominal slit widths, ranging from 130 - 190 µm due to divergence. Agreement between the methods was found for peak-to-valley dose ratio (PVDR), peak to peak separation and FWHM, but a difference in relative intensity of the microbeams was observed between the detectors.

Conclusions: The investigation demonstrated that pixelated CMOS sensors could be applied to microbeam radiotherapy for real-time dosimetry in the future, however the relatively large pixel pitch of the vM1212 detector limit the immediate application of the results.

1. INTRODUCTION

1A. Microbeam Radiotherapy

Microbeam radiotherapy (MRT) is a novel type of spatially fractionated therapy which is defined by narrow beams of radiation (typically < 100 µm) that can selectively irradiate portions of the target volume [1]. To cover the entire target volume, microbeams are delivered in a grid pattern in which multiple quasi-parallel rectangular beams, with typical centre-to-centre distances of 200 - 400 µm. Crucially the entire target volume is not irradiated uniformly, with regions of very high dose microbeam "peaks" separated by very low dose valleys.

Preclinical studies have indicated that this dose pattern has a greater efficacy than that of a single uniform field [2]. Whilst the exact mechanism for preferential effect tumour is not fully understood and is likely a combination of effects. Possible mechanisms under investigation are preferential damage to vascular tissue in tumours[3–5], and radiation-induced bystander and abscopal effects [6,7].

1B. Current Verification Methods

The very small size and high dose gradients of microbeams present a significant challenge to most standard detectors. That combined with high dose rates at synchrotrons adds to the complexity when working towards accurate dosimetry for microbeam radiotherapy.

Stereotactic radiotherapy treatments (with radiation fields sizes typically between 0.4 - 30 mm[8]) have strict requirements on the geometrical and dosimetric accuracy from dose calculations to delivery of

19 ± 5% (k=2)[9]. Microbeam irradiations are a step forward in terms of complexity and at present there is no

20 dosimetry protocol or recommendations for dosimetry of irradiations with such beam configurations[10].

21 Much of the ongoing research in the community is dedicated to optimising irradiation

22 configurations in order to obtain the best therapeutic outcomes, with peak to peak distance[11], full-

23 width at half maximum (FWHM)[12] and the peak-to-valley dose ratio (PVDR)[13,14] being of particular

24 interest.

25 Due to the very small scales involved in microbeam radiotherapy, conventional radiotherapy

26 equipment for beam profile acquisition (like small volume ionisation chambers) are unable to resolve the

27 individual microbeam peaks [9]). Scanning other types of small volume detectors through a microbeam

28 peak has been previously performed with success by using a MOSFET dosimeter [15,16] or with a

29 commercial PTW (Physikalisch-Technische Werkstätten GmbH, Freiburg, Germany) microdiamond

30 detector[17], with resolutions of 1 μm[18]. This method has shown good agreement with radiochromic

31 film[19], however the measurements are acquired point by point and therefore the shape of the profiles

32 are not shown instantaneously which limits its use for *in vivo* dosimetry or *in situ* verification. The same

33 applies to the use of scintillating fibres, as shown by Archer *et al.*[20].

34 Various groups have developed silicon strip detectors capable of quantifying parameters of the

35 microbeam field [21–23]. Whilst hybrid strip detectors (with separate sensor and readout) can offer

36 greater resistance to radiation than monolithic pixelated detectors, strip detectors do not provide

37 detailed information about the 2D profile of the radiation field and, therefore, will be more sensitive to

38 angular misalignment.

39 A method of obtaining 2D relative dose distributions of microbeams was developed by Bartzsch *et*

40 *al*. [24] using optical microscopy and EBT3 films [25], which when using a microscope is technically

41 capable of spatial resolutions better than 1 μm. Due to film grain inhomogeneities this is reduced to 5 μm

42 in practise. This method builds on existing techniques for film dosimetry. Radiochromic films have a

43 relatively large dose range (0.5 to 20 Gy for EBT3[26]), however the analysis process is slow, requiring a

44 minimum of 24 hours for self-development post-irradiation [27]. At lower dose levels (less than 0.1

45 Gy[28,29]) noise becomes more significant. This typically necessitates two separate sets of irradiations for

46 the same set of microbeams, in order to be able to increase the accuracy of the assessment of the dose

47 distribution in the regions with lower dose range (valleys) without saturating the high dose region of the

48 microbeam peaks.

49 This investigation was carried out to evaluate the suitability of the newly developed vM1212 detector

50 for its use in the analysis of preclinical radiotherapy microbeams, using the custom built multi-slit

51 collimator at the Helmholtz Zentrum München, Germany. The objective was to quantify microbeam

52   parameters and to compare to results of the analysis of the same deliveries to EBT3 films, using the
53   optical microscopy method[24].

54   ## 2. MATERIALS AND METHODS

55   ### 2A. vM1212 Pixelated Detector

56   The vM1212 pixelated detector is a large format CMOS (complementary metal–oxide–
57   semiconductor) imaging sensor with 50 μm pixel pitch originally designed for medical and scientific x-ray
58   imaging by the CMOS Sensor Design Group at the Rutherford Appleton Laboratory [30] and is now
59   licenced and manufactured into a full detector assembly by vivaMOS Ltd. The active area of the vM1212
60   detector is approximately 6 x 6 cm^2 (1204 x 1248 pixels) and is sufficiently large to capture the entire
61   radiation field of the microbeam multislit collimator in a single instance.

62   The small pixel pitch and predicted resistance to damage caused by high levels of ionising
63   radiation justified a proof of principle investigation to determine the response of the detector to
64   microbeam radiation.

65   ### 2B. Methodology

66   A SARRP (Small Animal Radiation Research Platform) x-ray irradiator at the Helmholtz Zentrum
67   München was used for this investigation. The irradiation parameters were set to 220 kVp (0.67 mm Cu
68   HVL); 2.8 mA; and fine focus (effective beam source size of 0.4 mm[31]).

69   The tungsten microbeam multislit collimator consisted of three levels of fifty one 100-μm slits (7 mm
70   total thickness), with a slit-to-slit separation of 400 μm. The first and third level are in a fixed alignment,
71   whilst the second central level is controlled by two motorised translation stages. When fully open, the
72   transmission gap is 100 μm, but the finest step resolution of the piezoelectric pistons enables variable slit
73   widths between 0 - 100 μm to be investigated to an accuracy of 0.5 μm. The collimator was mounted at a
74   distance of 21.2 cm from the source, with additional lead shielding to prevent radiation damage to the
75   electronics as shown in Figure 1a.

76   In order to obtain robust and safe positioning, the vM1212 detector had to be mounted at a
77   source to surface distance (SSD) of 29 cm, 6.8 cm from the surface of the microbeam collimator. To
78   achieve conditions similar to the ones used for small animal irradiations a 1 cm slab of tissue-equivalent
79   flexible bolus material with density of 1.03 g/cm [32] (trimmed to 7 x 7 cm^2) was placed on top of the
80   EBT3 film. The vM1212 detector was used without scintillating material to maximise the potential spatial
81   resolution. To enable a direct comparison between the EBT3 film and the vM1212 detector, EBT3 film

82 pieces were placed on top of the active area of the sensor, separated by a thin layer of a non-fibrous card

83 which had been marked for repeatable alignment (Figure 1b).

84 The EBT3 films irradiated simultaneously to the vM1212 detector were scanned using an Epson

85 Expression 10000XL flatbed scanner (1400 dpi) and calibrated using FilmQA Pro with triple channel

86 dosimetry[33,34]. Due to time constrains during the experiment, it was not possible to irradiate a second

87 set of films for their analysis with optical microscopy. Those irradiations were performed in an

88 independent experiment following the same irradiation conditions: source-surface distance, same bolus

89 material and non-fibrous card, but using 450 µm of silicon simulating the thickness of the detector. This

90 second set of films was scanned using a ZEISS Axio Imager 2 optical microscope[35] on 5X magnification

91 for a pixel resolution of 1.29 µm.

92 Prior to the film irradiations, the output (Gy/min) was measured in reference conditions for

93 SARRP absolute calibration. Measurements were performed with the SARRP open field at Source Surface

94 Distance (SSD) of 33 cm and at 2 cm depth in WT1 water equivalent slab phantom, with 3 cm of

95 backscatter material. Two independent measurements of the SARRP output were performed, one with

96 the local dosimetry system (PTW 30010 ionisation chamber), traceable to the PTW-Freiburg SSDL

97 Calibration Laboratory and with a National Physical Laboratory (NPL) secondary standard system (PTW

98 30012 ionisation chamber), traceable to the NPL primary standard for medium energy x-rays. Both

99 ionisation chambers used a local PTW Unidos TW1001 electrometer for dosimetry. Following output

100 measurements and in order to obtain a calibration curve, a set of nine films were irradiated in the same

101 reference conditions, with doses ranging from 0 to 14 Gy.

102 For consistency throughout the investigation, the same integration time, 28 ms, was always used

103 on the vM1212 detector. This ensured that all the performed measurements were all in the linear

104 response region for the pixels and prevented saturation of the detector. The results obtained using the

105 vM1212 detector were corrected by averaging over a number of frames to reduce noise, subtracting a

106 dark image to account for dark current in the pixels and calibrating the pixel response values against

107 measurements with the NPL ionisation chamber under the same conditions.

108 Direct comparison between the EBT3 films and the different acquisitions with vM1212 detector

109 were carried out for 25, 50, 75 and 100 µm slit widths. All the slits were irradiated with 240 s of exposure

110 with the exception of the 25 µm slit width which was irradiated with 480 s, to increase the dose and

111 therefore to reduce the level of noise for the films measurements in such narrow beams.

112 Finally, to understand the difference in spatial response between the vM1212 detector and the

113 two methods of EBT3 film scanning, the modulation transfer function (MTF) was measured for each. The

114 modulation transfer function of the vM1212 detector was measured following BS EN 62220-1-3:2008 [36]

115 and using the COQ analysis software written by Donini *et al.* [37]. The MTF of the Epson Expression
116 10000XL scanner at 1400 dpi scanning resolution was measured using a sharp flat edge positioned over a
117 piece of unexposed EBT3 film at an angle of 4°. Again using the COQ analysis software, the edge spread
118 function was calculated allowing the modulation transfer function to be determined. The MTF of the Zeiss
119 Axio Imager 2 was measured with the Xradia resolution sample (provided by Zeiss), which contained a
120 pattern of lines with known width and separation. The largest line width on this pattern was 32 μm
121 (period = 64 μm), and as such the smallest resolution measurable with this resolution sample was 15.6
122 line pairs/mm (1/0.064 mm).

123 ## 3.   RESULTS

124 ### 3A. Profile measurements

125 It was found that the vM1212 detector was able to capture the entire radiation field as defined by
126 the collimator, as can be seen in Figure 2b. To create the microbeam collimator slits in tungsten, 0.3 mm
127 diameter holes had to be drilled into the tungsten, allowing for wire erosion to mill out the 100 μm wide
128 slits. This detail can be recognized on both detectors (film and vM1212 detector) and was used for
129 alignment purposes. All profile comparisons presented are aligned relative to the central 26th peak. By
130 comparing vertical profiles from the EBT3 film methods with vertical profiles taken using the vM1212
131 detector we were able to observe that the alternating pattern of peaks and valleys of the microbeam
132 collimator are well correlated between the different detectors. The larger SSD required to mount the
133 vM1212 detector and the maximum scanning size of the EBT3 film possible with the microscope reduced
134 the number of peaks that could be recorded using this method to approximately 40 (reduced from 51
135 physical slits on the collimator).

136 The 100 μm slit profiles' comparison can be seen in Figure 3a, where an agreement in terms of
137 alignment of the peaks between the three detector methods can be observed. The vM1212 detector and
138 the Epson Expression 10000XL under respond in terms of peak dose by approximately 30% however there
139 is relatively good agreement of the location of the microbeam peak centre values (Figure 3b). As shown in
140 Figure 4, relative to the Zeiss Axio Imager 2, the valley doses are over reported by the Epson Expression
141 10000XL (with scanning resolution at 1400 dpi) by approximately 25% (15 mGy/min), whilst the vM1212
142 detector over reports by less than 5% (5 mGy/min). The average deviation between corresponding peak
143 centres for the vM1212 detector and the Epson Expression 10000XL measurement was 18.5 μm, whilst for
144 the Zeiss Axio Imager 2 measurement was found to be 55.3 μm. As shown in Figure 5 for the 26th central
145 peak, the profile resolved on all three detector methods appears to be Gaussian.

146   For the 25 μm slit width comparison (Figure 6) the agreement between the EBT3 films and the

147   vM1212 detector becomes worse as there is a strong disagreement for dose rate values between the scan

148   performed by the Zeiss Axio Imager 2 and the other methods. This deviation is likely due to spatial

149   averaging within the vM1212 detector and the Epson Expression 10000XL, however it is also possible that

150   this deviation was introduced by misalignment during the Zeiss Axio Imager 2 exposure as it was

151   performed at a later date. The lower measured dose rate is not consistent across the microbeam profiles

152   as shown for the central peak (Figure 8), where the dose rate measured by the vM1212 detector and

153   Epson Expression 10000XL EBT3 film is approximately 20% of the dose rate measured by the Zeiss Axio

154   Imager 2. For the Epson Expression 10000XL and the vM1212, the dose rate measured for the 27th peak

155   (Figure (9) is better but still measures only 40% relative to the Zeiss Axio Imager 2. Valley profiles for the

156   25 μm slit measured all of the detectors are again inconsistent, with approximate differences relative to

157   the Zeiss Axio Imager 2 of 40% and 20% for the vM1212 detector and Epson Expression 10000XL,

158   respectively. This peak specific under response not observed in the Zeiss Axio Imager 2 measurement is

159   suspected to be due to a combination of manufacturing tolerances on the machined microbeam slits and

160   repeatability issues of the microbeam setup.

161   Figures 8 and 9 show a profile comparisons with a Gaussian fit applied between the three

162   detectors for the 26th (central) and 27th peak, respectively. A stitching artefact between the high dose

163   valley irradiation and the low dose peak measurement can been seen in Figure 9 in the Zeiss Axio Imager

164   2 dose profile at approximately 50 μm. The centres of the 27th microbeam peak (relative to the 26th

165   central peak) can be calculated to be 550, 514 and 488 μm for the vM1212 detector, Epson Expression

166   10000XL and Zeiss Axio Imager 2 respectively.

167   The peak to peak separation could be measured across the three detection methods for all

168   measured slit widths, as shown in Table 1. It can be shown that the three methods agree within the

169   uncertainties calculated. Using the inverse square law and the differences between the measured peak to

170   peak separations, it can be estimated that the EBT3 films for the Epson Expression 10000XL and Zeiss Axio

171   Imager 2 measurements were positioned 0.5 ± 0.2 mm and 2.4 ± 0.2 mm closer respectively to the x-ray

172   source than the vM1212 detector measurement. As the measurements for the Epson Expression 10000XL

173   were taken concurrently with the vM1212 detector, this difference can be attributed to the thickness the

174   non-fibrous card which was independently measured with a digital calliper to be 0.53 ± 0.01 μm. The 2.4

175   mm deviation of the Zeiss Axio Imager 2 measurement is likely due to setup misalignment.

176   It was also found that the vM1212 detector was still able to detect and identify each of the 51

177   peaks when the microbeam collimator is fully closed (set to 0 μm slit width) (Figure 10). Profiles resulting

178   from this leakage are used in sections 3B FWHM measurements and 3C Peak and Valley Measurements.

179   Using the vM1212 detector it is possible to take real time horizontal profiles of the microbeam

180   collimator. A comparison between the methods averaged across all recorded peaks for the 100 μm slit

181   width can be seen in Figure 11, which again shows the approximately 30% under response of the vM1212

182   detector and Epson Expression 10000XL measurements relative to the Zeiss Axio Imager 2 measurement.

183   The sharp vertical peaks at 13,000 and 41,000 μm are due to the 0.3 mm diameter holes seen in Figure 2.

184   It can be seen in all three methods that the radiation intensity does not follow a smooth profile across the

185   collimator as one might expect, although it is beyond the scope of this paper to discuss any therapeutic

186   impact this may have.

187   **3B. FWHM measurements**

188   An averaged FWHM comparison between the Zeiss Axio Imager 2 and the vM1212 detector for

189   each of the slits can be seen in Figure 12. The error bars shown represent one standard deviation of

190   uncertainty for the microbeam peaks.

191   A linear relationship between the FWHMs is observed however there is a large deviation between

192   FWHMs within a measurement. This can be attributed to a significant trend in the FWHM as a function of

193   vertical position that was undetectable at the time of the experiment that can be seen in both the

194   vM1212 detector results (Figure 13) and the analysed EBT3 films (not shown). This is most probably due

195   to the angle of the beam after it is produced at the tungsten target, within the x-ray tube, known as heel

196   effect. This effect would have become more dominant due to the larger SSD and was not observed on

197   past measurements using the microbeam collimator.

198   Such a difference in beam FWHM across the beam profile would have had a significant impact on

199   patient outcome, as described by Serduc *et al.* [12]. For *in vivo* verification this would have been

200   impossible to diagnose in real time with EBT3 films, due to the minimum 24 hour time required for film

201   self-development. This highlights a potential application of the vM1212 detector for real time imaging of

202   microbeams.

203   A comparison of microbeam nominal slit width to the measured FWHM can be seen in Figure 14.

204   As the vM1212 detector could take multiple readings with minimal dead time between them, a repeat set

205   of measurements was performed to calculate the FWHM of the microbeams. Each time the slit width was

206   increased by 5 μm. Using this approach, it was possible to show that below 20 μm slit width, the value of

207   the measured FWHM begins to increase (in relation to the expected nominal one). This effect is well

208   documented for small fields in megavoltage x-ray beams[38] and is due to the finite size of the x-ray

209   source being partially occluded by the collimator, causing an overlapping beam penumbra. If this

210   geometrical penumbra is larger than the field size, then the FWHM of the resulting beam increases.

211   Differences between the two vM1212 detector measurements are attributed to subtle differences when

212   repositioning the detector and uncertainties in the reproducibility of the collimator movements, however

213   this effect appears to be minimal.

214   The larger FWHM for all measurements can be attributed to the finite size of the x-ray source. As

215   shown in Figure 15, for a finite source size (S), collimator slit width (w), source-collimator distance (A), and

216   collimator-projection distance (B); the projected beam width can be approximated using equation (1).

217
$$L = \left[\frac{B}{A} + 1\right]w + \frac{BS}{A} \text{ (1)}$$

218   For this approximation and to simplify the scatter effects, we assumed that the collimator is infinitely thin

219   and consists of only one layer instead of the three that comprise the actual and previously described

220   design of the collimator. With the previous assumptions we are considering the calculated projected

221   beam size as an approximation of the FWHM of the microbeam peak.   Using the values described

222   previously for A, B and S, the values for the theoretical resolvable slit size were plotted on Figure 14 for

223   comparison with measured results. With equation 1, the smallest microbeam peak FWHM created by the

224   collimator that could be possible to resolve would be equal to 128.3 ± 13.0 µm (assuming 10% uncertainty

225   of x-ray source size), whilst using the extrapolated results from the vM1212 detector the minimum is

226   calculated to be 126.0 ± 0.7 µm. The differences in the slope between the derived (geometric

227   approximation) and measured (vM1212 detector repeat linear fit) FWHMs are likely to be due to the

228   numerous approximations and would need full Monte Carlo simulation with an accurate model of the

229   geometry and scatter conditions.

230   **3C. Peak and Valley Measurements**

231   By fitting Gaussians to each of the peaks in both the vM1212 detector and EBT3 film profiles, the

232   Peak-to-Valley Dose Ratio (PVDR) can be estimated and compared to results reported in the literature

233   (Figure 16). The values calculated for the PVDR were comparable to what one might expect for this

234   microbeam collimator when comparing to previous measurements in a similar collimator by Bartzsch *et*

235   *al.* (where 15.5 ± 1.5 was measured at 10 mm depth) [39], especially when considering the significantly

236   larger SSD of this investigation.

237   The PVDRs obtained using the Epson Expression 10000XL for the 25 and 50 µm slit widths were

238   found to be significantly larger than both predicted by literature and as reported by the vM1212 detector

239   and the Zeiss Axio Imager 2 measurements. This can be attributed to a significant under response of the

240   Epson Expression 10000XL to the microbeam valleys, as shown in Figure 7. It is possible that the two film

241   method used for optical microscopy could be applied to compensate for this and record a more accurate

242   dose profile, however this was not within the scope of the investigation.

243   Using the vM1212 detector it was possible to rapidly calculate the PVDR for a large number of slit

244   widths. As shown in Figure 10, radiation leak is present through the collimator at slit width 0 μm from

245   which a PVDR could be calculated. The decrease in PVDR below 20 μm is consistent with the increase in

246   FWHM as observed in Figure 14 which was attributed to an increased proportion of the radiation resulting

247   from scatter with decreasing slit width.

248   3D. Modulation Transfer Measurements

249   The results of modulation transfer measurements are shown in Figure 17. It can be shown that while

250   the spatial resolution of the vM1212 detector is better than the Epson Expression 10000XL scanner, the

251   Zeiss Axio Imager 2 microscope is superior to both.

252

253   4. DISCUSSION

254   In comparison to dedicated facilities such as the European Synchrotron Radiation Facility (ESRF), the

255   x-ray source used for this investigation was not optimised for microbeam radiotherapy with the dose rate

256   measured after the collimator to be less than 0.05 Gy/s. This is substantially less than the dose rate used

257   at synchrotrons for microbeam radiotherapy (often exceeding 100 Gy/s)[40]. The microbeam FWHMs

258   delivered in this investigation are significantly larger than the 25 μm wide beams capable at the ESRF and

259   as such, further research of the vM1212 detector under such beam conditions is required. The mean

260   energy of this investigation (approximately 95 keV as calculated by the x-ray emission spectra calculation

261   software SpekCalc[41–43]) was comparable to that of dedicated synchrotrons[44,45], however

262   undoubtedly the effect of the different spectra must be considered.

263   A comparison of the three microbeam detection methods evaluated in this work can be seen in Table

264   2. Whilst the vM1212 detector has demonstrated the feasibility of a CMOS sensor for microbeams

265   measurement in this investigation, significant deviations to established dosimetry methods were

266   observed and further studies comparing to Monte Carlo simulations for relative dosimetry are still

267   necessary. The Zeiss Axio Imager 2 remains a suitable readout method for commissioning and situations

268   where maximum precision is required however, this method is relatively young and validated protocols

269   and workflows need to be established to allow wider uptake for this method among microbeam

270   community. The use of the Epson Expression 10000XL for microbeam measurements is not recommended

271   due to the (relatively) poor spatial resolution.

272   The vM1212 detector does not possess the spatial resolution necessary for accurate microbeam

273   dosimetry with its relatively large 50 μm pixels, compared to other quality assurance mechanisms

274   discussed previously (such as the PTW microdiamond) with ~ 1 μm resolution. In addition, well

275   established characteristics of other detection methods necessary for routine quality assurance such as

276   dose rate and beam quality dependence have not been taken into account. The vM1212 detector

277   operates using a "rolling shutter" frame acquisition method which does not present an issue for static or

278   slow moving microbeam sources such as the type used in this investigation but may not be ideal for fast

279   scanned microbeam spots. Additionally the maximum full field refresh rate of 34 fps may cause temporal

280   blurring, however this effect could be minimised by binning pixels together or recording only a smaller

281   region of interest. This refresh rate is still considerably lower than that of commercial radiotherapy

282   electrometers (such as the Unidos webline with 1 kHz sampling rate[46]). Whilst the dose delivered to the

283   films scanned by the Epson Expression 10000XL is relatively low (average peak dose of > 1 Gy) for EBT3

284   film standards, it must be noted that the vM1212 detector is capable of obtaining similar or better quality

285   images in less than 2 mGy per frame, highlighting its potential for real-time microbeam verification.

286   Looking forward, CMOS sensors resistant to ionising radiation have been developed for other harsh

287   radiation environments (such as space), achieving pixel pitches of less than 10 µm [47,48] in size. The use

288   of such sensors in the future could obtain real-time microbeam profile information surpassing even that

289   of the Zeiss Axio Imager 2, however making these sensors large enough to cover the same field of view as

290   the vM1212 detector could become prohibitively expensive due the number of pixels required and sensor

291   yield losses.

292   ## 5. CONCLUSION

293   Microbeam radiotherapy is a rapidly developing method of cancer treatment with significant

294   therapeutic improvements over conventional radiotherapy [50,51]. The dosimetric challenges associated

295   with the high dose gradients in microbeam radiotherapy prevent the use of well-established dosimetry

296   equipment used in radiotherapy and (to date), all novel techniques for monitoring microbeams have only

297   obtained one dimensional profile information; limiting their clinical viability.

298   In this study we have demonstrated the capacity of the two dimensional vM1212 pixelated detector

299   to discriminate individual microbeams peaks with FWHM between 130 and 190 µm. The high dynamic

300   range of the vM1212 detector allows the signal detection of both the high dose peaks and the low dose

301   valleys (of microbeams with less than 20 PVDR) to be measured in real-time, which provides a significant

302   advantage over EBT3 films requiring at least 24 hours post-irradiation processing. Observed peak-to-valley

303   dose ratios and peak to peak separations measured by the vM1212 detector were comparable those

304   obtained using the optical microscopy method employing Zeiss Axio Imager 2 microscope. The use of

305   pixelated sensors for in-*vivo* beam monitoring in conventional radiotherapy beams is already being

306 researched by multiple groups[52,53] and as the technology behind the sensors matures, it is anticipated
307 that future CMOS detectors will have all of the required characteristics for microbeam dosimetry.
308

309 ## ACKNOWLEDGMENT

315 ## CONFLICT OF INTEREST DISCLOSURE

316 Due to the prototype nature of the device, the manufacturer of the vM1212 detector, vivaMOS
317 Ltd, has been involved in data collection providing advice and technical support throughout the
318 investigation.
319

320 a) Author to whom correspondence should be addressed. sam.flynn@npl.co.uk

321

322 [1] Slatkin D N, Spanne P, Dilmanian F A and Sandborg M 1992 Microbeam radiation therapy *Med. Phys.* **19** 1395–400
323 [2] Bouchet A, Serduc R, Laissue J A and Djonov V 2015 Effects of microbeam radiation therapy on normal and tumoral
324 blood vessels *Phys. Medica* **31** 634–41
325 [3] Serduc R, Christen T, Laissue J, Farion R, Bouchet A, Sanden B van der, Segebarth C, Bräuer-Krisch E, Le Duc G, Bravin A,
326 Rémy C and Barbier E L 2008 Brain tumor vessel response to synchrotron microbeam radiation therapy: a short-term *in*
327 *vivo* study *Phys. Med. Biol.* **53** 3609–22
328 [4] Crosbie J C, Anderson R L, Rothkamm K, Restall C M, Cann L, Ruwanpura S, Meachem S, Yagi N, Svalbe I, Lewis R A,
329 Williams B R G and Rogers P A W 2010 Tumor Cell Response to Synchrotron Microbeam Radiation Therapy Differs
330 Markedly From Cells in Normal Tissues *Int. J. Radiat. Oncol.* **77** 886–94
331 [5] Bouchet A, Serduc R, Laissue J A and Djonov V 2015 Effects of microbeam radiation therapy on normal and tumoral
332 blood vessels *Phys. Medica* **31** 634–41
333 [6] Prise K M, Schettino G, Folkard M and Held K D 2005 New insights on cell death from radiation exposure *Lancet Oncol.* **6**
334 520–8
335 [7] Fernandez-Palomo C, Bräuer-Krisch E, Laissue J, Vukmirovic D, Blattmann H, Seymour C and Mothersill C 2015 Use of
336 synchrotron medical microbeam irradiation to investigate radiation-induced bystander and abscopal effects in vivo *Phys.*
337 *Medica* **31** 584–95
338 [8] Bagheri H, Soleimani A, Gharehaghaji N, Mesbahi A, Manouchehri F, Shekarchi B, Dormanesh B and Dadgar H 2017 An
339 overview on small-field dosimetry in photon beam radiotherapy: Developments and challenges *J. Cancer Res. Ther.* **13**

340   175

341 [9]   Das I J, Downes M B, Kassaee A and Tochner Z 2000 Choice of Radiation Detector in Dosimetry of Stereotactic
342   Radiosurgery-Radiotherapy *J. Radiosurgery* **3** 177–86

343 [10]   Bräuer-Krisch E, Serduc R, Siegbahn E A, Le Duc G, Prezado Y, Bravin A, Blattmann H and Laissue J A 2010 Effects of
344   pulsed, spatially fractionated, microscopic synchrotron X-ray beams on normal and tumoral brain tissue *Mutat. Res. -*
345   *Rev. Mutat. Res.* **704** 160–6

346 [11]   Regnard P, Le Duc G, Bräuer-Krisch E, Troprès I, Siegbahn E A, Kusak A, Clair C, Bernard H, Dallery D, Laissue J A and
347   Bravin A 2008 Irradiation of intracerebral 9L gliosarcoma by a single array of microplanar x-ray beams from a
348   synchrotron: Balance between curing and sparing *Phys. Med. Biol.* **53** 861–78

349 [12]   Serduc R, Bouchet A, Bräuer-Krisch E, Laissue J A, Spiga J, Sarun S, Bravin A, Fonta C, Renaud L, Boutonnat J, Siegbahn E
350   A, Estève F and Le Duc G 2009 Synchrotron microbeam radiation therapy for rat brain tumor palliation—influence of the
351   microbeam width at constant valley dose *Phys. Med. Biol.* **54** 6711–24

352 [13]   Bräuer-Krisch E, Adam J-F, Alagoz E, Bartzsch S, Crosbie J, DeWagter C, Dipuglia A, Donzelli M, Doran S, Fournier P, Kalef-
353   Ezra J, Kock A, Lerch M, McErlean C, Oelfke U, Petasecca M, Povoli M, Rosenfeld A, Siegbahn E A, Sporea D and Stugu B
354   2015 Medical physics aspects of the synchrotron radiation therapies: Microbeam radiation therapy (MRT) and
355   synchrotron stereotactic radiotherapy (SSRT) *Phys. Medica* **31** 568–83

356 [14]   Annabell N, Yagi N, Umetani K, Wong C and Geso M 2012 Evaluating the peak-to-valley dose ratio of synchrotron
357   microbeams using PRESAGE fluorescence *J. Synchrotron Radiat.*

358 [15]   Rosenfeld A B, Kaplan G I, Kron T, Allen B J, Dilmanian A, Orion I, Ren B, Lerch M L F and Holmes-Siedle A 1999 MOSFET
359   dosimetry of an X-ray microbeam *IEEE Trans. Nucl. Sci.* **46** 1774–80

360 [16]   Kaplan G I, Rosenfeld A B, Allen B J, Booth J T, Carolan M G and Holmes-Siedle A 2000 Improved spatial resolution by
361   MOSFET dosimetry of an x-ray microbeam *Med. Phys.* **27** 239–44

362 [17]   Livingstone J, Stevenson A W, Butler D J, Häusermann D and Adam J F 2016 Characterization of a synthetic single crystal
363   diamond detector for dosimetry in spatially fractionated synchrotron x-ray fields *Med. Phys.* **43** 4283–93

364 [18]   PTW Freiburg 2013 IONIZING RADIATION DETECTORS: Including Codes of Practice 100

365 [19]   Rosenfeld A B 2006 Electronic dosimetry in radiation therapy *Radiat. Meas.* **41** S134–53

366 [20]   Archer J, Li E, Davis J, Cameron M, Rosenfeld A and Lerch M 2019 High spatial resolution scintillator dosimetry of
367   synchrotron microbeams *Sci. Rep.* **9** 6873

368 [21]   Lerch M L F, Dipuglia A, Cameron M, Fournier P, Davis J, Petasecca M, Cornelius I, Perevertaylo V and Rosenfeld A B 2017
369   New 3D Silicon detectors for dosimetry in Microbeam Radiation Therapy *J. Phys. Conf. Ser.* **777** 012009

370 [22]   Davis J A, Paino J R, Dipuglia A, Cameron M, Siegele R, Pastuovic Z, Petasecca M, Perevertaylo V L, Rosenfeld A B and
371   Lerch M L F 2018 Characterisation and evaluation of a PNP strip detector for synchrotron microbeam radiation therapy
372   *Biomed. Phys. Eng. Express* **4** 044002

373 [23]   Povoli M, Alagoz E, Bravin A, Cornelius I, Bräuer-Krisch E, Fournier P, Hansen T-E E, Kok A, Lerch M, Monakhov E, Morse
374   J, Petasecca M, Requardt H, Rosenfeld A B, Röhrich D, Sandaker H, Salomé M and Stugu B 2015 Thin silicon strip
375   detectors for beam monitoring in Micro-beam Radiation Therapy *J. Instrum.* **10** P11007–P11007

376 [24]   Bartzsch S, Lott J, Welsch K, Bräuer-Krisch E and Oelfke U 2015 Micrometer-resolved film dosimetry using a microscope
377   in microbeam radiation therapy *Med. Phys.* **42** 4069–79

378 [25]   Anon *GAFCHROMIC ™ DOSIMETRY MEDIA, TYPE EBT-3*

379 [26]   Anon Garchromic EBT Films - GAFchromic™

380 [27] McLaughlin W L, Yun-Dong C, Soares C G, Miller A, Van Dyk G and Lewis D F 1991 Sensitometry of the response of a new
381   radiochromic film dosimeter to gamma radiation and electron beams *Nucl. Instruments Methods Phys. Res. Sect. A Accel.*
382   *Spectrometers, Detect. Assoc. Equip.* **302** 165–76

383 [28] Li Y, Chen L, Zhu J and Liu X 2017 The combination of the error correction methods of GAFCHROMIC EBT3 film *PLoS One*
384   **12** 1–17

385 [29] Tagiling N, Ab Rashid R, Azhan S N A, Dollah N, Geso M and Rahman W N 2018 Effect of scanning parameters on dose-
386   response of radiochromic films irradiated with photon and electron beams *Heliyon* **4** e00864

387 [30] Sedgwick I, Das D, Guerrini N, Marsh B and Turchetta R 2013 LASSENA: A 6.7 Megapixel, 3-sides Buttable Wafer-Scale
388   CMOS Sensor using a novel grid- addressing architecture *Proc. Int. Image Sens. Work.* 3–6

389 [31] Tryggestad E, Armour M, Iordachita I, Verhaegen F and Wong J W 2009 A comprehensive system for dosimetric
390   commissioning and Monte Carlo validation for the small animal radiation research platform. *Phys. Med. Biol.* **54** 5341–57

391 [32] Anon ExaFlex™ - MacroMedics

392 [33] Micke A, Lewis D F and Yu X 2011 Multichannel film dosimetry with nonuniformity correction *Med. Phys.* **38** 2523–34

393 [34] Mayer R R, Ma F, Chen Y, Miller R I, Belard A, McDonough J and O'Connell J J 2012 Enhanced dosimetry procedures and
394   assessment for EBT2 radiochromic film *Med. Phys.* **39** 2147–55

395 [35] Anon ZEISS Axio Imager 2 for Life Science Research

396 [36] Anon 2015 *BSI Standards Publication Medical electrical equipment — Characteristics of digital x-ray imaging devices Part*
397   *1-1 : Determination of the detective quantum efficiency — Detectors used in*

398 [37] Donini B, Rivetti S, Lanconelli N and Bertolini M 2014 Free software for performing physical analysis of systems for
399   digital radiography and mammography

400 [38] Das I J, Ding G X and Ahnesjö A 2007 Small fields: Nonequilibrium radiation dosimetry *Med. Phys.* **35** 206–15

401 [39] Bartzsch S, Cummings C, Eismann S and Oelfke U 2016 A preclinical microbeam facility with a conventional x-ray tube
402   *Med. Phys.* **43** 6301–8

403 [40] Eling L, Bouchet A, Nemoz C, Djonov V, Balosso J, Laissue J, Bräuer-Krisch E, Adam J F and Serduc R 2019 Ultra high dose
404   rate Synchrotron Microbeam Radiation Therapy. Preclinical evidence in view of a clinical transfer *Radiother. Oncol.* **139**
405   56–61

406 [41] Poludniowski G G and Evans P M 2007 Calculation of x-ray spectra emerging from an x-ray tube. Part I. Electron
407   penetration characteristics in x-ray targets *Med. Phys.* **34** 2164–74

408 [42] Poludniowski G G 2007 Calculation of x-ray spectra emerging from an x-ray tube. Part II. X-ray production and filtration
409   in x-ray targets *Med. Phys.* **34** 2175–86

410 [43] Poludniowski G, Landry G, DeBlois F, Evans P M and Verhaegen F 2009 *SpekCalc* : a program to calculate photon spectra
411   from tungsten anode x-ray tubes *Phys. Med. Biol.* **54** N433–8

412 [44] Martínez-Rovira I, Sempau J and Prezado Y 2012 Development and commissioning of a Monte Carlo photon beam model
413   for the forthcoming clinical trials in microbeam radiation therapy *Med. Phys.* **39** 119–31

414 [45] Livingstone J, Stevenson A W, Häusermann D and Adam J-F 2018 Experimental optimisation of the X-ray energy in
415   microbeam radiation therapy *Phys. Medica* **45** 156–61

416 [46] PTW 2010 *User Manual: UNIDOS webline Type 10021, Type 10022 and Type 10023*

417 [47] Sellier C, Gambart D, Perrot N, Garcia-Sanchez E, Virmontois C, Mouallem W and Bardoux A 2019 Development and
418   qualification of a miniaturised CMOS camera for space applications (3DCM734/3DCM739) *International Conference on*
419   *Space Optics — ICSO 2018* vol 11180, ed N Karafolas, Z Sodnik and B Cugny (SPIE) p 106

420 [48] Kim W T, Park C, Lee H, Lee I and Lee B G 2019 A high fullwell capacity CMOS image sensor for space applications
421 *Sensors (Switzerland)* **19**

422 [49] Borca V C, Pasquino M, Russo G, Grosso P, Cante D, Sciacero P, Girelli G, Porta M R La and Tofani S 2013 Dosimetric
423 characterization and use of GAFCHROMIC EBT3 film for IMRT dose verification *J. Appl. Clin. Med. Phys.* **14** 158

424 [50] Schültke E, Balosso J, Breslin T, Cavaletti G, Djonov V, Esteve F, Grotzer M, Hildebrandt G, Valdman A and Laissue J 2017
425 *Microbeam radiation therapy-grid therapy and beyond: a clinical perspective*

426 [51] Prezado Y, Jouvion G, Patriarca A, Nauraye C, Guardiola C, Juchaux M, Lamirault C, Labiod D, Jourdain L, Sebrie C,
427 Dendale R, Gonzalez W and Pouzoulet F 2018 Proton minibeam radiation therapy widens the therapeutic index for high-
428 grade gliomas *Sci. Rep.* **8** 16479

429 [52] Page R F, Abbott N L, Davies J, Dyke E L, Randles H J, Velthuis J J, Fletcher S, Gregory S D, Hall C, John A M, Lawrence H,
430 Stevens P H, Hugtenburg R P and Tunbridge V 2014 Using a monolithic active pixel sensor for monitoring multileaf
431 collimator positions in intensity modulated radiotherapy *IEEE Trans. Nucl. Sci.* **61** 74–8

432 [53] Bartoli A, Scaringella M, Baldi A, Greto D, Scoccianti S, Masi L, Pallotta S, Bruzzi M and Talamonti C 2018 PO-0873: 2D
433 pixelated diamond detector for patient QA in advanced radiotherapy treatments *Radiother. Oncol.* **127** S459–60

434

Figure 1: Experimental set up: (a) vM1212 detector with 1 cm of water equivalent build-up, (b) vM1212 detector with aligned EBT3 Film.
  i.   Lead shield to protect collimator electronics
  ii.   Microbeam collimator
  iii.   1 cm of water equivalent bolus
  iv.   Cable for microbeam collimator
  v.   vM1212 detector
  vi.   Ribbon cables for vM1212 detector
  vii.   Non-fibrous card with alignment points
  viii. 3 x 3 cm^2 square of EBT3 film

Figure 2: (a) Photograph of microbeam collimator slits. (b) vM1212 detector image (cropped). (c) Scan of exposed EBT3 film using the Epson Expression 10000XL scanner (100 μm slit width). (d) Scan of exposed EBT3 film using Zeiss Axio Imager 2.

Figure 3: (a) 100 μm slit width profile comparison, (b) Microbeam peak deviation between the vM1212 detector and the two EBT3 film methods.

Figure 4: 100 μm slit width valley profile comparison.

Figure 5: 100 μm slit width profile comparison of the 26th central peak.

Figure 6: 25 μm slit width profile comparison.

Figure 7: 25 μm slit width valley profile comparison.

Figure 8: 25 μm slit width peak profile comparison of the 26th central peak.

Figure 9: 25 μm slit width peak profile comparison of the 27th peak.

Figure 10: Radiation leakage through the collimator at 0 μm slit width as measured by the vM1212 detector.

Figure 11: Horizontal profile of the 100 μm slit width.

Figure 12: FWHM comparison between Zeiss Axio Imager 2 and the vM1212 detector. A 1:1 ratio has been added to guide the eye.

Figure 13: FWHM trend as measured by the vM1212 detector.

Figure 14: Comparing the microbeam slit width to observed FWHM.

Figure 15: Geometric setup of the microbeam collimator, resulting in the larger full width at half maximum (FWHM).

Figure 16: Comparison of PVDR for different slit widths. The PVDR measurements for the 25 and 50 μm slit width Epson Expression 10000XL are omitted.

Figure 17: Comparison of MTF for different measurement techniques.

Table 1: Measured peak to peak separation as measured on the three detectors. Statistical uncertainty corresponds to one standard deviation.

	Measured peak to peak separation (µm)		
Nominal slit width (µm)	vM1212 detector	Epson Expression 10000XL	Zeiss Axio Imager 2
25	513.4 ± 13.9	512.0 ± 11.3	508.3 ± 9.9
50	512.9 ± 10.1	511.7 ± 9.7	508.9 ± 9.1
75	512.6 ± 9.2	511.9 ± 10.1	508.3 ± 8.6
100	512.4 ± 9.5	511.8 ± 9.6	508.5 ± 9.8

Table 2: Comparison of the different microbeam detection methods evaluated in this work.

	Microbeam detection method		
	vM1212 detector	**Zeiss Axio Imager 2 (+ EBT3 film)**	**Epson Expression 10000XL (+ EBT3 film)**
Advantages	Real time measurement and analysis	Highest spatial resolution	Lower cost
	Short exposure is sufficient to obtain accurate profile information	No dose rate dependence[49]	Established clinical workflow
			No dose rate dependence[49]
Disadvantages	Limited life expectancy due to cumulative radiation damage	24 hours self-development	24 hours self-development
	Spatial resolution limited by 50 µm pixel pitch	Complex and time consuming analysis process	Poorest spatial resolution ad hence limited suitability for microbeam applications
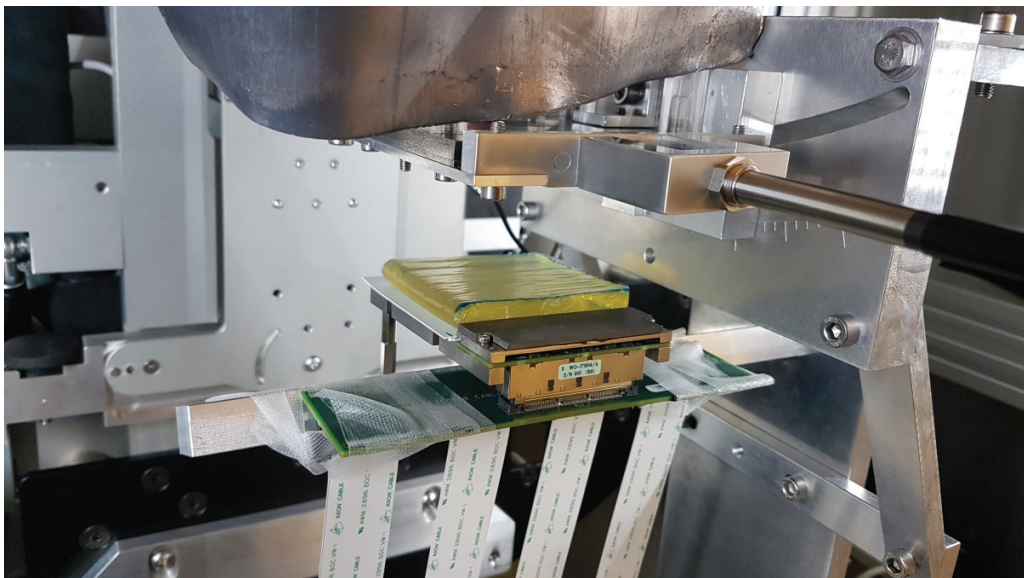
mp_13971_f1a.tif
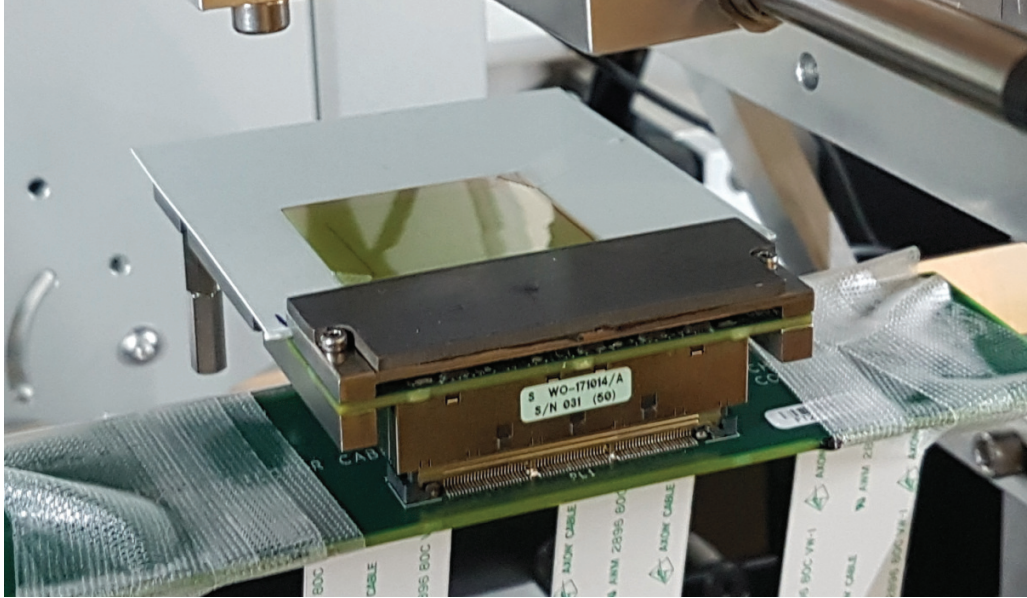
mp_13971_f1b.tif
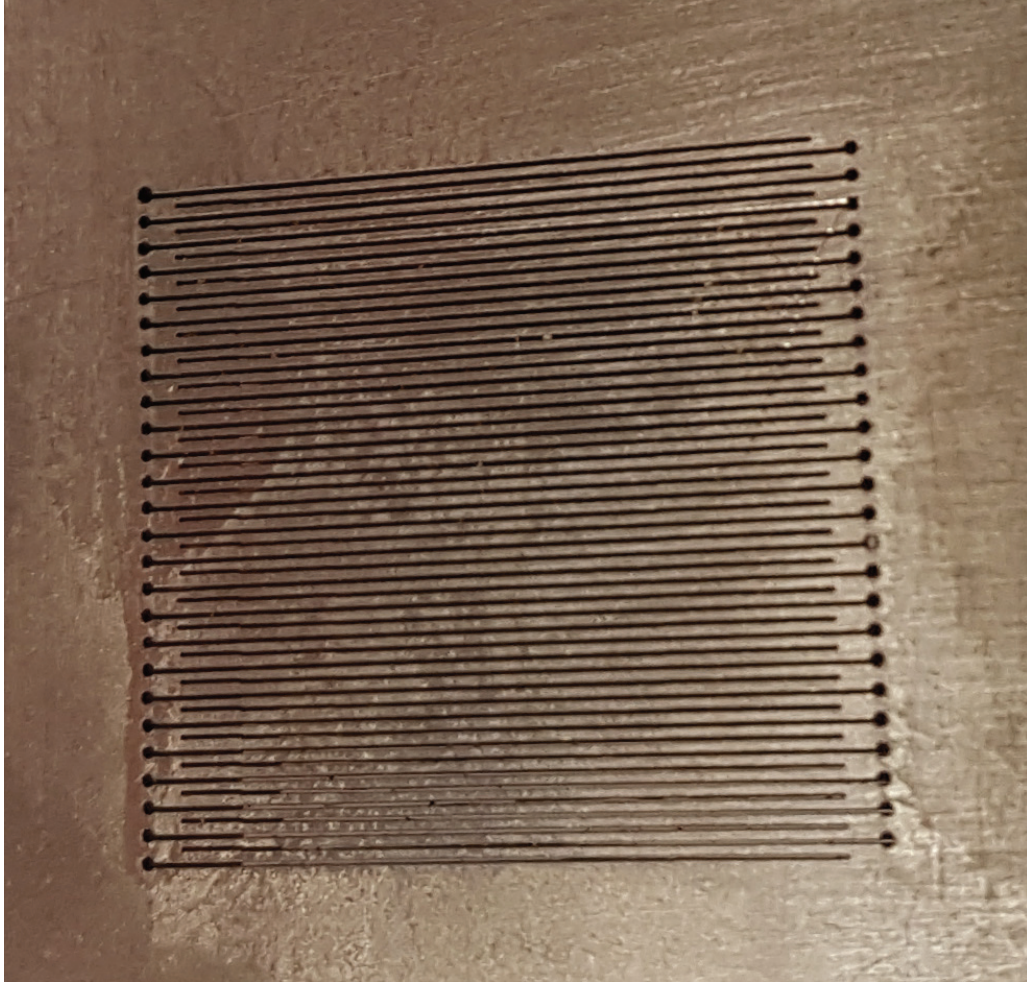
mp_13971_f2a.tif
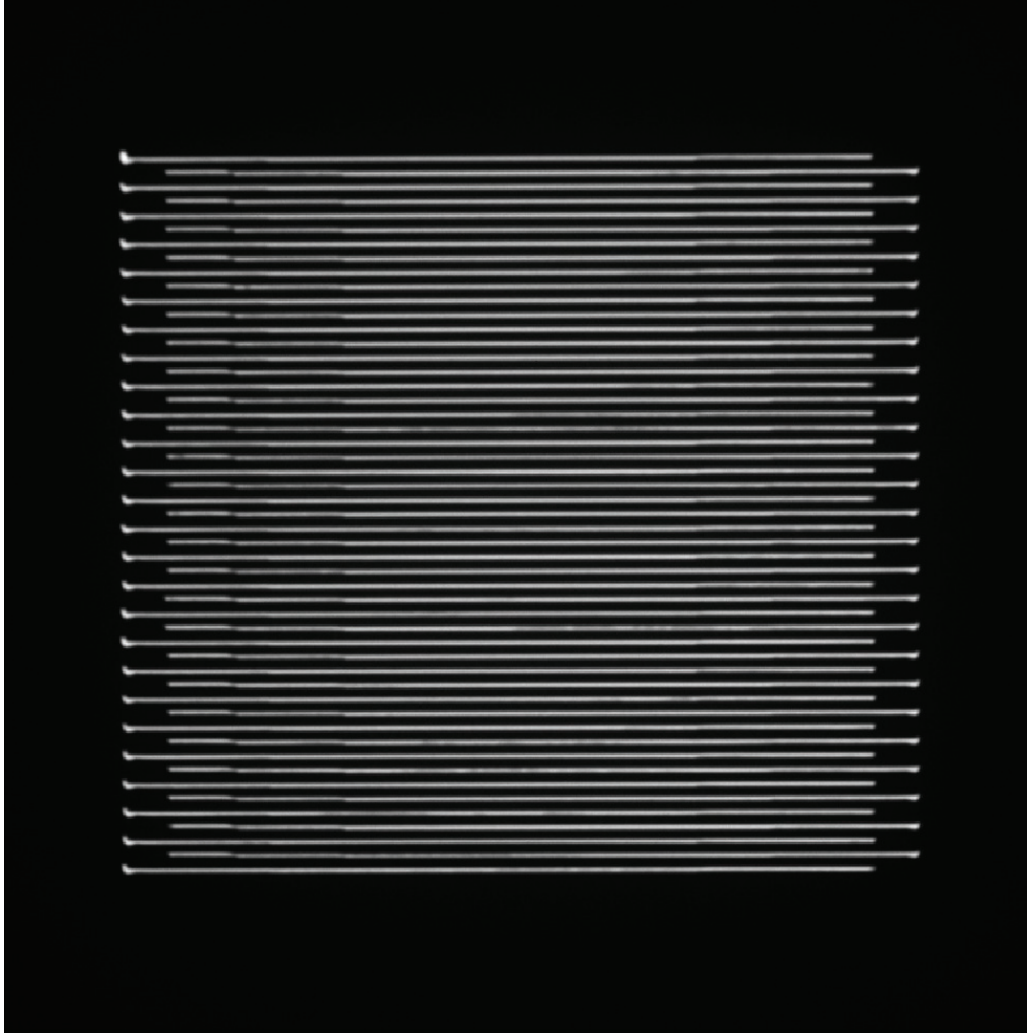
mp_13971_f2b.tif

mp_13971_f2c.tif
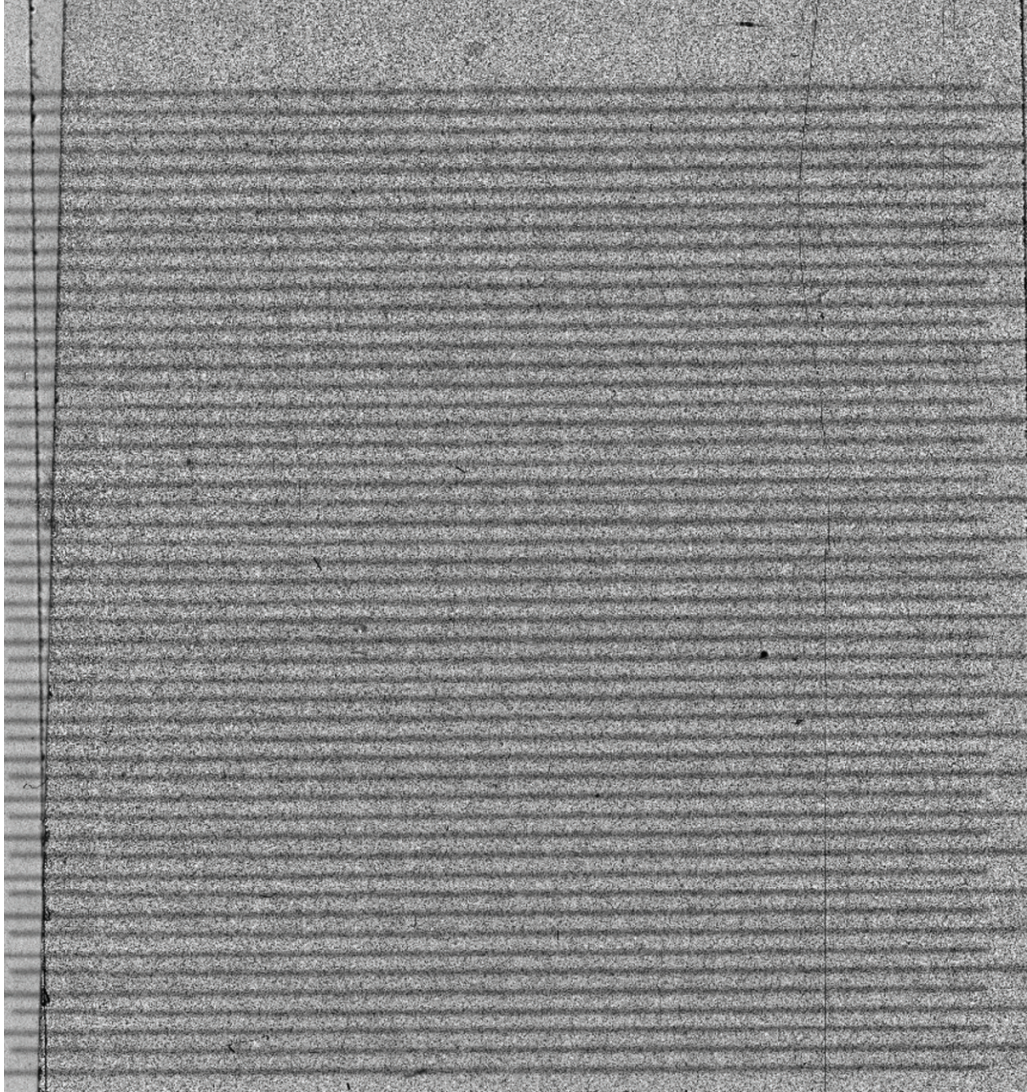
mp_13971_f2d.tif
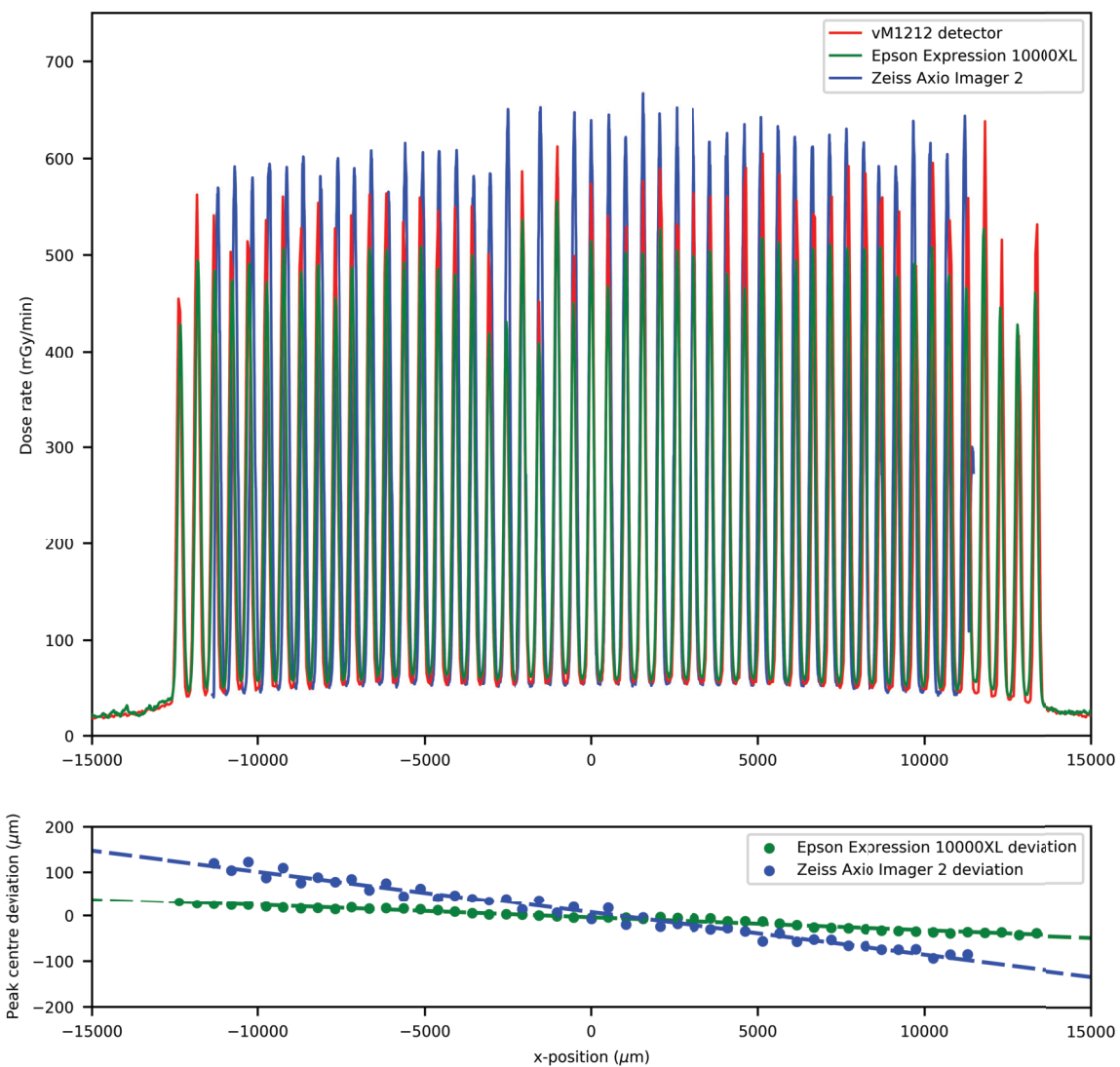
mp_13971_f3.tif
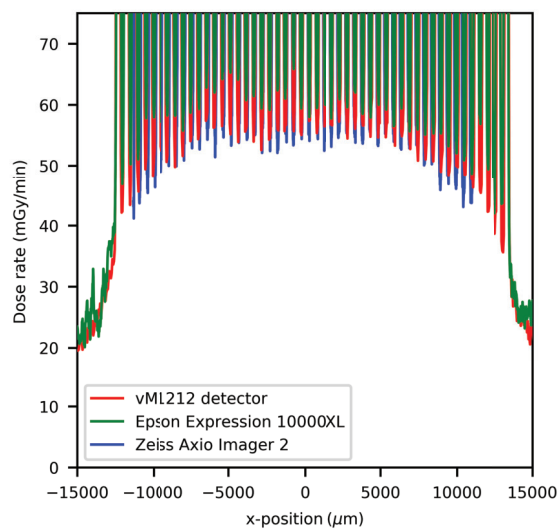
mp_13971_f4.tif
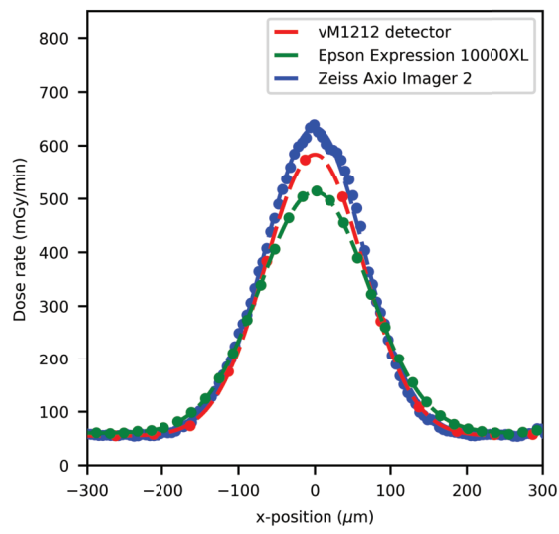
mp_13971_f5.tif
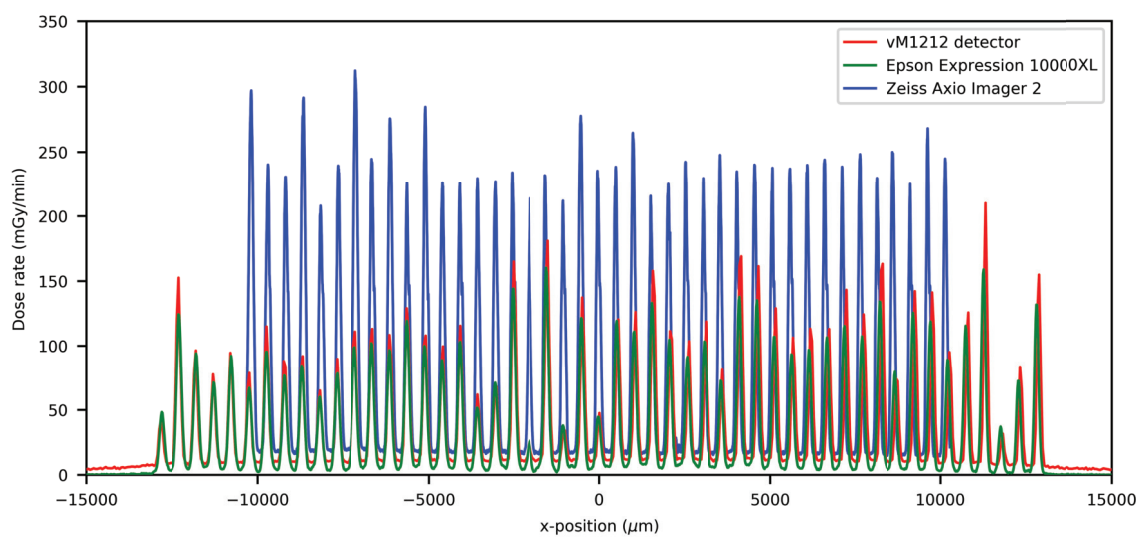
mp_13971_f6.tif
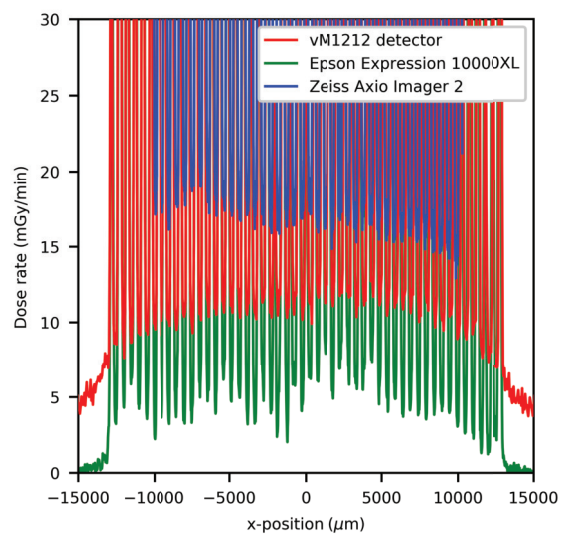
mp_13971_f7.tif
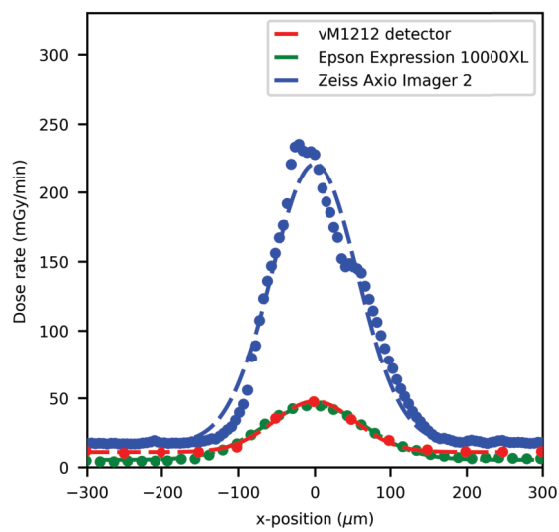
mp_13971_f8.tif
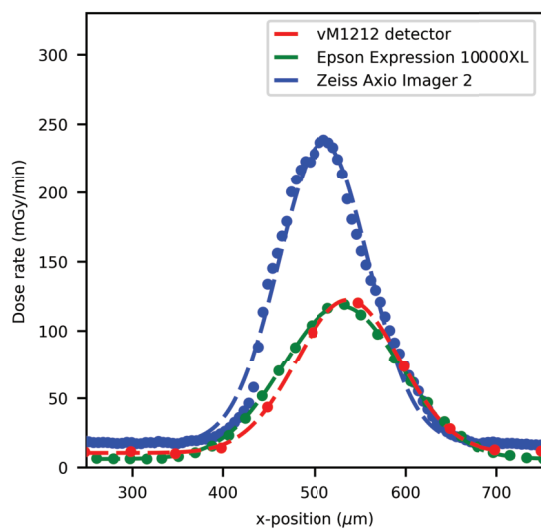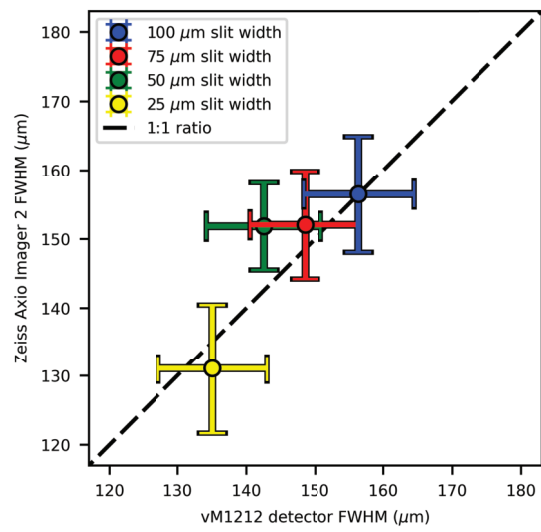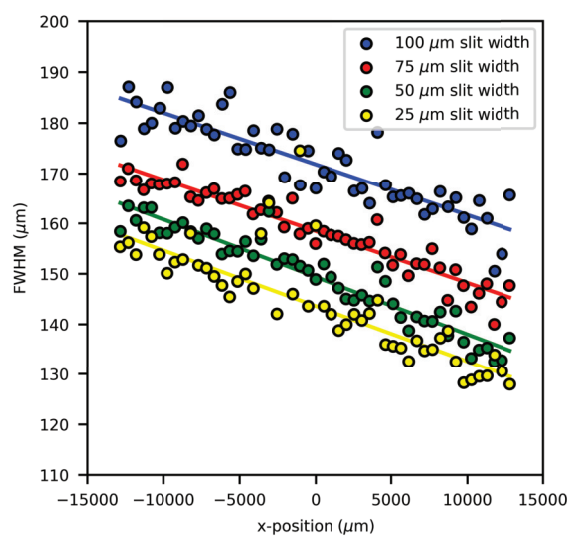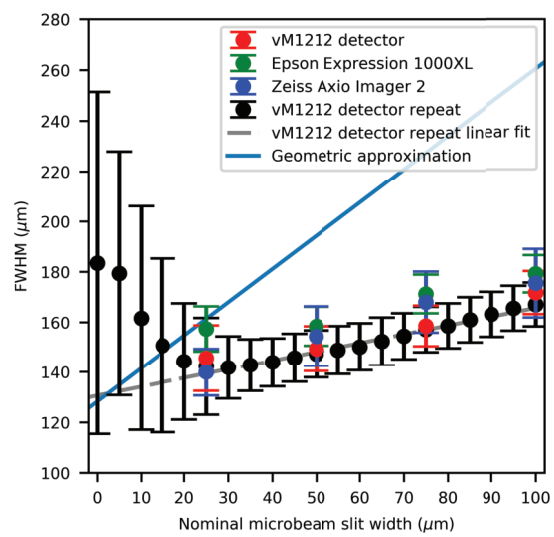
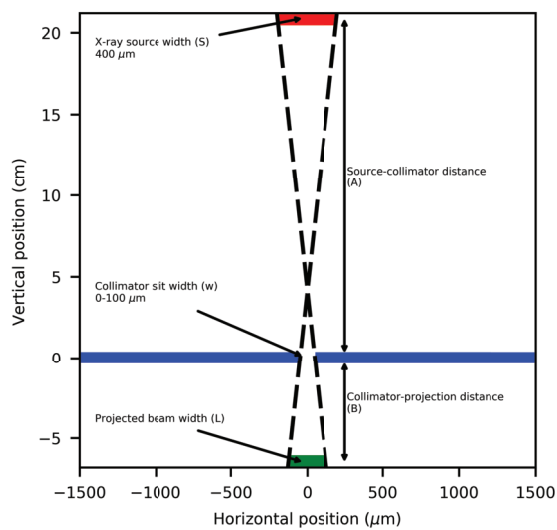mp_13971_f9.tif
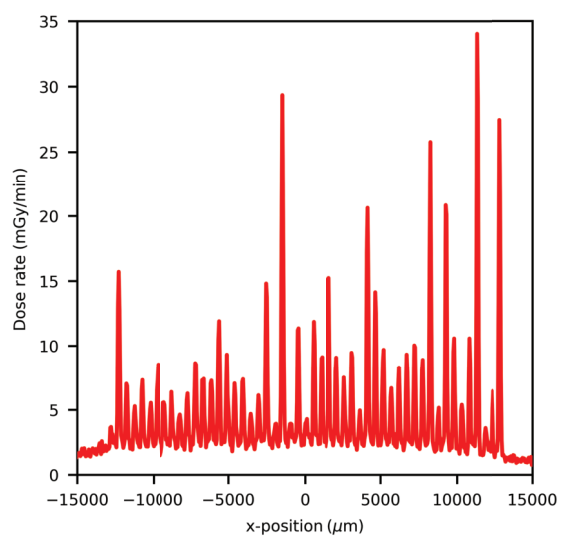
mp_13971_f10.tif
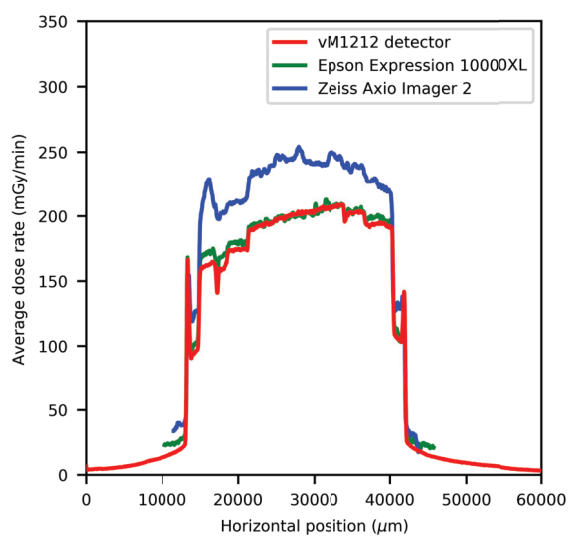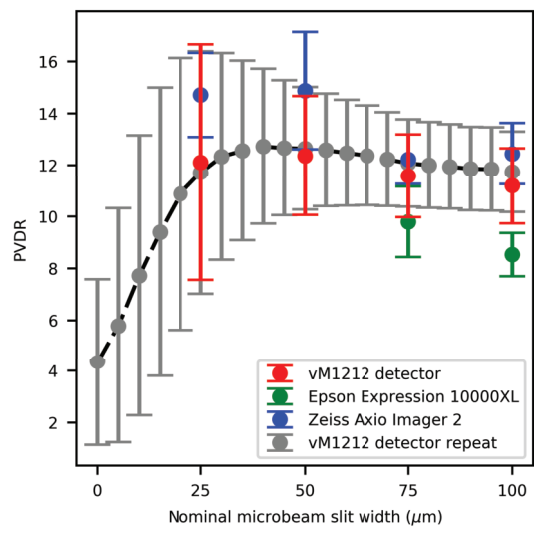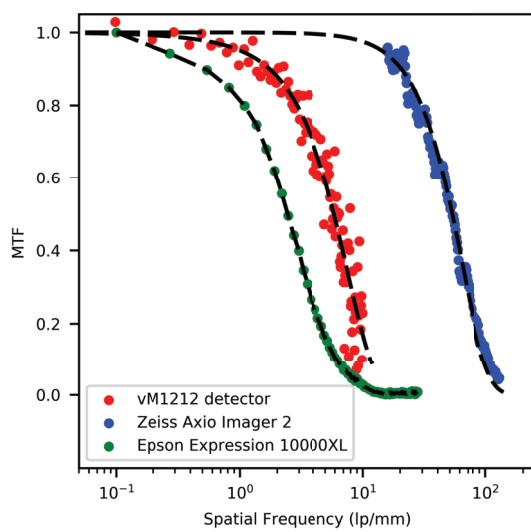
mp_13971_f11.tif

mp_13971_f12.tif

mp_13971_f13.tif

mp_13971_f14.tif

mp_13971_f15.tif

mp_13971_f16.tif

mp_13971_f17.tif